Global energy transfer during a magnetospheric field line resonance

Michael Hartinger,[1] Vassilis Angelopoulos,[1] Mark B. Moldwin,[1,2] Karl-Heinz Glassmeier,[3] and Yukitoshi Nishimura[4,5]

Received 18 April 2011; accepted 4 May 2011; published 18 June 2011.

[1] Field line resonances (FLRs) are important for transferring energy from fast mode waves to shear Alfvén waves in the Earth's magnetosphere. Using simultaneous multi-satellite observations from THEMIS and the IMAGE ground magnetometer array, we report on the transfer of energy from compressional magnetopause undulations through an FLR to the ionosphere. Energy diversion from the magnetosphere to the ionosphere took place at the FLR: we find net energy flux there to have comparable values in the radial and the field-aligned directions. The field-aligned energy flux, when mapped to the ionosphere, was 0.70 mW/m^2 and consistent with the inferred Joule dissipation rate at that time. IMAGE's regional monitoring of wave activity reveals that the temporal evolution of the FLR wave power and energy transfer were correlated with the amplitude profile of magnetopause undulations, confirming these waves to be the FLR driver. **Citation:** Hartinger, M., V. Angelopoulos, M. B. Moldwin, K.-H. Glassmeier, and Y. Nishimura (2011), Global energy transfer during a magnetospheric field line resonance, *Geophys. Res. Lett.*, *38*, L12101, doi:10.1029/2011GL047846.

1. Introduction

[2] The Earth's magnetosphere is an inhomogeneous medium. This facilitates energy transfer between different plasma wave modes at plasma boundaries. Early models of magnetohydrodynamic (MHD) wave propagation in Earth's magnetosphere suggested that the shear and compressional MHD wave modes could couple via a field line resonance (FLR) mechanism [*Tamao*, 1965]. Energy transfer near an FLR has been modeled in several studies [e.g., *Junginger*, 1985; *Kouznetsov and Lotko*, 1995]. If the FLR is being driven by a source in the solar wind or a surface wave at the magnetopause, net energy flux directed earthward into the resonance region is expected. This energy flux is both kinetic and electromagnetic (Poynting vector). Electromagnetic energy transfer will be the focus of this study; however, it should be noted that kinetic energy flux can significantly alter the expected behavior of the MHD wave modes associated with field line resonance [*Kouznetsov and Lotko*, 1995]. In the FLR region, the earthward energy flux is converted to net field-aligned energy flux, as the FLR loses energy to the ionosphere through Joule dissipation [*Newton et al.*, 1978; *Glassmeier et al.*, 1984]. It is expected that earthward energy flux (perpendicular to the background magnetic field) should be larger near the magnetic equator, as models and observations show that compressional MHD waves are confined to this region [*Zhu and Kivelson*, 1991; *Lee*, 1996].

[3] *Junginger et al.* [1985] examined the Poynting vector for Pc5 pulsations, finding values from 10^{-10} to 10^{-5} W/m^2 that were often directed radially inward and tailward. *Rae et al.* [2005] identified a specific FLR that was steady over several hours and using ground and satellite measurements they examined the associated Poynting vector averaged over several wave cycles. They found that the radial Poynting vector component was smallest, followed by a significant azimuthal (tailward) and a dominant field-aligned component. *Rae et al.* [2007] examined the energy balance between the average field-aligned Poynting vector and Joule dissipation rate in the ionosphere, finding that they were nearly equal.

[4] The goal of this study is to examine the energy transfer associated with a shear Alfvén mode generated through the FLR mechanism. We present simultaneous observations of an FLR near the magnetic equator (i.e., where compressional-to-shear Alfven wave coupling is strong), at the magnetopause boundary (i.e., where the solar wind driver imparts energy) and on the ground, where a network of stations removes the space-time ambiguity associated with single spacecraft crossings of a resonant L-shell. The fortuitous conjunction occurred on 31 October 2008 near the dawn terminator.

2. Instrumentation

[5] We use magnetospheric data from the five-satellite Timed History of Events and Macroscale Interactions (THEMIS) mission, solar wind data from OMNIweb that have been time-referenced to the subsolar magnetopause, and ground magnetometer data from the International Monitor for Auroral Geomagnetic Effects (IMAGE) array [*Sibeck and Angelopoulos*, 2008]. Observations from the five THEMIS satellites are particularly useful for ULF wave studies [e.g., *Agapitov et al.*, 2009; *Sarris et al.*, 2010]. Each satellite has a 3 second spin period and is equipped with a fluxgate magnetometer (FGM) [*Auster et al.*, 2008], an electric field instrument (EFI) [*Bonnell et al.*, 2008], and an ion and electron electrostatic analyzer (ESA) [*McFadden*

[1]Earth and Space Sciences Department, University of California, Los Angeles, California, USA.
[2]Atmospheric, Oceanic, and Space Sciences Department, University of Michigan, Ann Arbor, Michigan, USA.
[3]Institute for Geophysics and Space Physics, Technical University of Braunschweig, Braunschweig, Germany.
[4]Atmospheric and Oceanic Sciences Department, University of California, Los Angeles, California, USA.
[5]Solar-Terrestrial Environment Laboratory, Nagoya University, Toyokawa, Japan.

Copyright 2011 by the American Geophysical Union.
0094-8276/11/2011GL047846

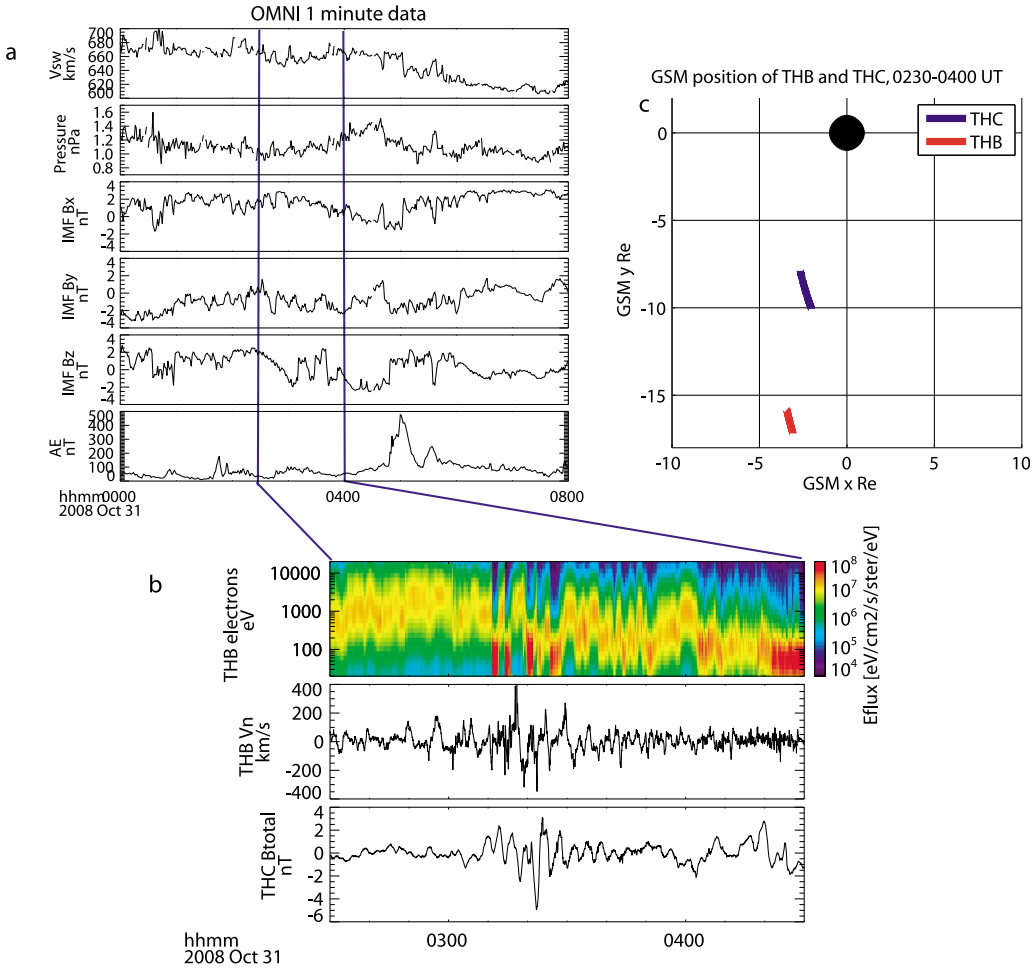

Figure 1. (a) From top to bottom, solar wind velocity, dynamic pressure, IMF Bx (GSE/GSM), IMF By (GSM), IMF Bz (GSM), and the AE index from OMNIweb. (b) From top to bottom, a dynamic energy flux spectrogram from TH-B (electrons), the plasma velocity component normal to the magnetopause inferred from TH-B ESA ion measurements, and detrended magnetic field magnitude from TH-C. (c) The orbits of TH-B and TH-C in the GSM equatorial plane during the interval from 0230 to 0400 UT.

et al., 2008]. EFI provides its highest-quality low frequency measurements in the spin-plane. The third component of the electric field is obtained by assuming E*B = 0 when the normal of the spacecraft spin plane is sufficiently far from the background magnetic field direction. ESA measures the three-dimensional particle distributions and moments (electrons: 5 eV–30 keV, ions 5eV–25 keV) once per spin.

3. Observations

[6] The FLR event occurred during a period of quiet geomagnetic activity, elevated (~650 km/s) solar wind velocity, weak dynamic pressure, and some IMF fluctuations (see Figure 1a, top). The high value of the solar wind speed suggests that the magnetopause was most probably Kelvin-Helmholtz unstable [e.g., *Engebretson et al.*, 1998]. Magnetopause undulations were observed by THEMIS-B (TH-B, P1) between 0230 to 0400 UT near the magnetopause boundary, as shown in Figure 1b: The energy-time spectrogram from ESA data (Figure 1b, top) shows the characteristic signatures of alternating hot (1 keV) magnetospheric and cold (100 eV) magnetosheath electrons, consistent with multiple magnetopause crossings. We follow *Liu et al.* [2008] and compute the component of the ion velocity (from ESA on board moments) normal to the nominal magnetopause. Several strong negative/positive excursions in the normal velocity occur inside the magnetopause just before/after sheath crossings in (Figure 1b, middle). These magnetopause velocity undulations have an approximate frequency of 5 mHz (as determined by the spacing between negative excursions) and clearly increase in amplitude from 0310 to 0330 UT. TH-C is located several Earth Radii (R_E) inside of the magnetopause (Figure 1c). The high-pass filtered (>0.5 mHz) total magnetic field at TH-C is shown in Figure 1b (bottom). ULF waves of about 5 mHz frequency, consistent with the velocity perturbations observed by TH-B, are evident there.

[7] Similarly high-pass filtered electric and magnetic field vectors observed at TH-C were rotated into a field-aligned coordinate system in which y points eastward, z is along the background magnetic field (direction obtained from low pass filtered data, frequency <0.5 mHz), and x completes the orthogonal set pointing approximately radially outward. In Figure 2a, the x component of the electric field is shown, and Figure 2b is for the corresponding dynamic power spectrum. A large enhancement in wave activity occurred

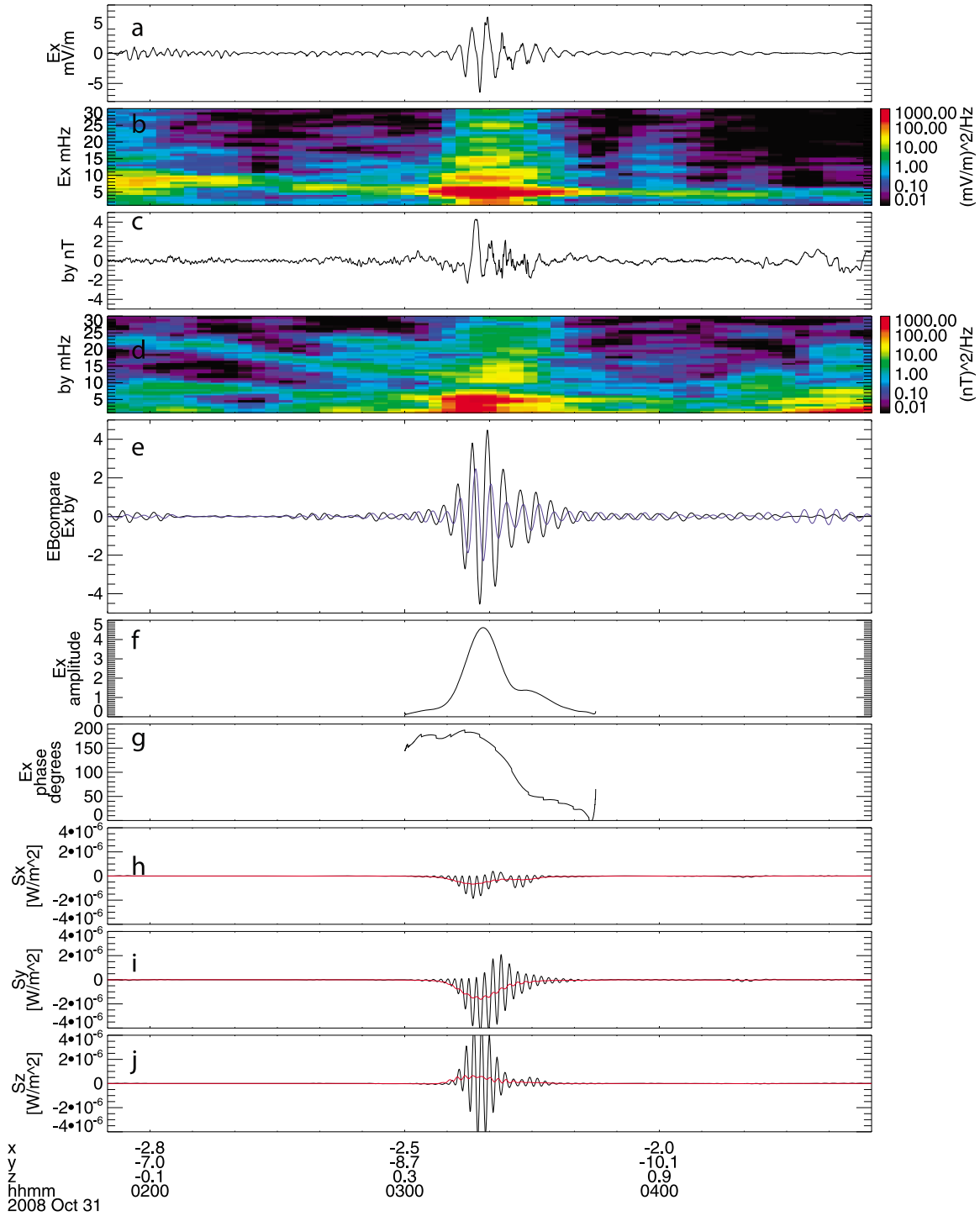

Figure 2. (a) Radial electric field, (b) radial electric field dynamic power spectra, (c) east–west magnetic field, (d) east–west magnetic field spectra, (e) band pass filtered (3–6 mHz) radial electric (black) and east–west magnetic field (blue) data, (f) instantaneous amplitude of radial electric field, (g) instantaneous phase of radial electric field, (h) radial Poynting vector (black) and time averaged radial Poynting vector (red), (i) east–west Poynting vector, and (j) field-aligned Poynting vector. The time average is computed with a running 10 minute boxcar window.

from 0310 to 0340 UT. The frequency of the enhanced wave activity was ~5 mHz, with several harmonics at higher frequencies. Figures 2c and 2d show the y component of the detrended magnetic field and corresponding dynamic power spectrum; an enhancement is also seen there at ~5 mHz.

[8] To examine the phase relations amongst various components we next band pass filter (3–6 mHz) these data and plot the radial electric and east–west magnetic field components in Figure 2e. It is evident that the electric and magnetic field were approximately 90 degrees out of phase during the period of enhanced wave activity. We next

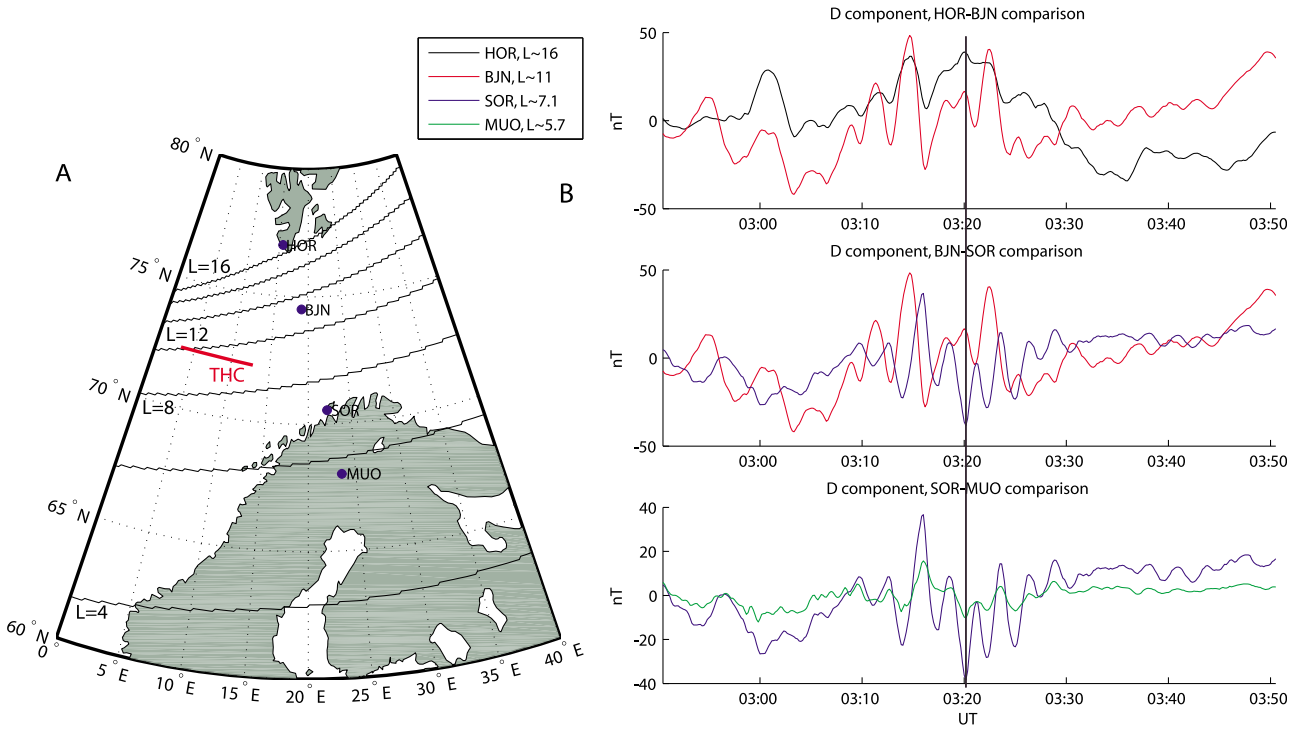

Figure 3. (a) The positions of IMAGE magnetometer stations are plotted on a geographic grid (dotted lines) and solid black lines of constant McIlwain L parameter are overplotted in steps of 2 Re. The red line is the ground track of TH-C, mapped from TH-C's position using field line tracing in the Mead and Fairfield magnetic field model. (b) In each panel, the H component of the magnetic field with hourly means subtracted is plotted for pairs of stations. The H component of the magnetic field observed at (top) HOR and BJN, (middle) BJN and SOR, and (bottom) SOR and MUO. A black line indicates a time when a 180 degree phase difference between BJN and SOR is particularly clear, whereas the other stations are in phase.

employ the method of the analytic signal to determine the instantaneous amplitude and phase of the x component of the electric field during the period of enhanced wave activity [*Glassmeier*, 1980]. Figures 2f and 2g show a clear change in phase of about 180 degrees across the amplitude peak. All of the observations presented in Figures 2a–2g are therefore consistent with a toroidal wave mode associated with an FLR: there was a localized peak in amplitude in both the radial electric and east–west magnetic field; the two field components were 90 degrees out of phase; there was a clear jump in phase of approximately 180 degrees across the FLR; and harmonics were observed. Finally, the frequency of 5 mHz is expected for a toroidal mode in this region [*Lee and Lysak*, 1989].

[9] Figures 2h–2j show, in black lines, the Poynting flux components computed using the band-pass filtered data in a field aligned coordinate system. Red lines are component running averages (10 minute window), showing the net energy transfer over several wave cycles. It is clear that the strongest energy flux in all three directions occurred at ~0310–0330 UT. Figure 2h shows the radial component, with a net energy flux towards Earth. The east–west component, in Figures 2i, shows a net energy flux westward, i.e., towards the magnetotail, given the spacecraft location at the dawn terminator. The field-aligned component, in Figure 2j, shows a net energy flux towards the northern ionosphere, as expected for a damped standing wave.

[10] Finally, we examine 10 sec magnetic field data from the IMAGE magnetometer array. The IMAGE magnetometers were in the same local time sector as TH-C at the time the FLR was observed (Figure 3a). To compare with TH-C observations, we overplot lines of constant L parameter [*McIlwain*, 1966], calculated at time 0315 UT using software from the French National Aerospace Research Center (ONERA). This McIlwain parameter, L, is a proxy of the equatorial distance of a ground point. We chose to use *Mead and Fairfield*'s [1975] external magnetic field model, combined with an International Geomagnetic Reference Field (IGRF), to compute these constant-L lines, because this combination provides the best match of the magnetic field at TH-B and TH-C during this interval. A red line shows the ground track of TH-C between 0300-0345 UT, mapped using the same model and software.

[11] The component of the magnetic field that points towards magnetic north, or H component, is shown in Figure 3b. The hourly mean is subtracted from these data, and data from two stations are overplotted in each panel. Figure 3b (top) is for the two stations at the highest magnetic latitudes, HOR and BJN, the next for intermediate latitudes, BJN and SOR, and the bottom for lowest latitudes, SOR and MUO. A 5 mHz signal is most clearly seen in the stations that map to locations close to THC (BJN and SOR), but this signal is also visible at other stations. A black line indicates a time when a 180 degree phase difference between BJN and SOR is clearly visible, whereas the other station pairs

have signals that are in phase. This phase jump at 5 mHz between BJN and SOR is apparent for several wave cycles and provides further confirmation that TH-C crossed through the center of an FLR, even though the FLR was evolving in time (see auxiliary material for additional dynamic power spectra and cross-phase spectrograms).[1] The observations at all four stations suggest that the wave activity increased after 0310 UT.

4. Discussion

[12] The FLR and associated wave activity observed by TH-C and ground magnetometers beginning at ~0310 UT appears to be strongly linked to the change in the character of the boundary undulations that occurred from ~0310–0330 UT. We conclude that the increase in amplitude of the magnetic field perturbations observed by TH-C beginning at 0310 UT was the result of the temporal evolution of the driver rather than the spatial motion of TH-C through the FLR. However, the rotation in phase of the radial electric field at TH-C (Figure 2g) and the phase variation observed by the ground magnetometers (Figure 3b and auxiliary material), argue that TH-C also fortuitously passed through the center of the FLR at approximately 0325 UT, i.e., approximately near the time of FLR absolute peak power.

[13] The average Poynting vector (from band pass filtered electric and magnetic field data, 3 to 6 mHz) observed by TH-C from 0310–0330 UT was $-4.3*10^{-7}$ W/m^2 for the radial component (earthward), $-8.6*10^{-7}$ W/m^2 for the azimuthal component (tailward), and $3.3*10^{-7}$ W/m^2 for the field-aligned component (towards the northern ionosphere). Net field-aligned energy flux was comparable to radial energy flux, suggesting that strong coupling was occurring between the driving wave and the Alfvèn waves via FLR.

[14] Our results differ from *Rae et al.* [2005], who observed "very small radial, significant azimuthal, and dominant field-aligned" Poynting vector near an FLR. In our case, the azimuthal component of the Poynting vector was the strongest for both net and instantaneous energy transfer. Additionally, the net radial Poynting vector was larger than the net field-aligned Poynting vector. Finally, the instantaneous radial Poynting vector was about 3 times larger relative to the instantaneous field-aligned Poynting vector in this study compared to *Rae et al.* [2005]. One potential explanation for these differences is the different positions of the satellites used in each study; *Rae et al.* [2005] used observations from POLAR, which was located between 4 and 15 degrees magnetic latitude, whereas TH-C was within 3 degrees of the magnetic equator (location determined using *Mead and Fairfield*'s [1975] model). Compressional MHD waves propagate near the magnetic equatorial plane, leading to higher perpendicular Poynting vectors in this region [*Zhu and Kivelson*, 1991; *Lee*, 1996]. Our observations suggest that TH-C is directly observing strong coupling between fast mode and shear Alfvén waves via FLR because of its location near the magnetic equator, as the observed radial and field-aligned energy transfer is comparable.

[15] The energy contained in the FLR region was gradually lost to the ionosphere through Joule dissipation [*Newton et al.*, 1978], manifested by the time-averaged energy flux towards the ionosphere. A positive net flux towards the northern ionosphere is expected near the magnetic equator when the conductivity is lower in the northern ionosphere (compared to the southern one) and the fundamental standing wave has a magnetic node at southern latitudes [*Allan*, 1982]. The Poynting flux from the FLR into the ionosphere should be comparable to Joule dissipation rates, if Joule dissipation is the primary damping mechanism for the shear Alfvén wave. Using IMAGE magnetometers, *Hardy et al.*'s [1987] statistical study of ionospheric conductivity, and the technique of *Ozeke et al.* [2009], we map the ground magnetic perturbation to an electric field in the ionosphere, Ei, and calculate the Joule dissipation rate using

$$W_{JD} = \Sigma_p |E_i|^2 \tag{1}$$

where Σ_p is the Pedersen conductivity [*Greenwald and Walker*, 1980]. We estimate a Joule dissipation rate of 0.16–1.0 mW/m^2, in good agreement with rates obtained from radar data in previous studies [*Greenwald and Walker*, 1980; *Rae et al.*, 2007]. See the auxiliary material for more details on this estimate.

[16] With regards to the Poynting flux, since TH-C passes through the center of the FLR between 0310–0330 UT, we use the time-averaged field-aligned Poynting vector from that interval to map to the ionosphere and compare it with estimates of the Joule dissipation rate. Assuming that the cross-sectional area of a flux tube is inversely proportional to the magnetic field strength we have:

$$\frac{S_2}{|B_2|} = \frac{S_1}{|B_1|} \tag{2}$$

where $|B_2|$ is the magnetic field strength observed on the ground, ~53000 nT, $|B_1|$ is the magnetic field strength at TH-C, ~25 nT, and S_1 is the time averaged Poynting vector observed from 0310 to 0330 UT by TH-C, $3.3*10^{-7}$ W/m^2. We thus find the energy flux into the ionosphere is S_2 = 0.70 mW/m^2. Evidently, the Joule dissipation rate obtained is between 23% and 150% of the energy flux into the ionosphere, both measured near the center of the FLR, implying that Joule dissipation is an important damping mechanism.

5. Summary and Conclusions

[17] The simultaneous, fortuitous crossing of a clearly identifiable FLR center by an equatorial THEMIS spacecraft, observation of the magnetopause by another spacecraft, and observation of the FLR on the ground by a regional network of magnetometers provides an opportunity to study the transfer of wave energy from compressional waves, to shear Alfvèn waves via FLR, and on to the ionosphere. The simultaneous observations of the solar wind, the magnetopause, and the FLR enable us to conclude that magnetopause surface waves are the source of energy for the FLR. The radial trajectory of TH-C near the magnetic equator allows us to quantify the energy transfer associated with the FLR in the radial ($-4.3*10^{-7}$ W/m^2) and field-aligned ($3.3*10^{-7}$ W/m^2) direction. These observations suggest a strong coupling between the fast mode waves driven

[1] Auxiliary materials are available in the HTML. doi:10.1029/2011GL047846.

at the magnetopause and the shear Alfvén waves via the FLR mechanism. Ground magnetometer observations demonstrate that TH-C crossed through the center of the FLR near the time that magnetopause undulations were the most pronounced and had the same frequency as the magnetospheric ULF waves. A comparison of the energy balance between the field-aligned energy flux observed by TH-C and the Joule dissipation rate in the ionosphere shows that Joule dissipation is an important damping mechanism.

[18] **Acknowledgments.** We acknowledge NASA THEMIS contract NAS5-02099; J. Bonnell and F. S. Mozer for use of the EFI data; and C. W. Carlson and J. P. McFadden for the use of the ESA data. We thank the NASA Space Science Data facility for use of solar wind data and models of CGM coordinates. We thank the creators of the ONERA-DESP software library. We thank the institutes that maintain the IMAGE magnetometer array. The work done by Karl-Heinz Glassmeier was financially supported by the German Ministerium für Wirtschaft und Technologie and the Deutsches Zentrum für Luft- und Raumfahrt under grant 50OC1001.

[19] The Editor thanks one anonymous reviewer for their assistance in evaluating this paper.

References

Agapitov, O., et al. (2009), Surface waves and field line resonances: A THEMIS case study, *J. Geophys. Res.*, *114*, A00C27, doi:10.1029/2008JA013553.

Allan, W. (1982), Phase variation of ULF pulsations along the geomagnetic field-line, *Planet. Space Sci.*, *30*(4), 339–346, doi:10.1016/0032-0633(82)90039-3.

Auster, H. U., et al. (2008), The THEMIS Fluxgate Magnetometer, *Space Sci. Rev.*, *141*(1–4), 235–264, doi:10.1007/s11214-008-9365-9.

Bonnell, J. W., F. S. Mozer, G. T. Delory, A. J. Hull, R. E. Ergun, C. M. Cully, V. Angelopoulos, and P. R. Harvey (2008), The Electric Field Instrument (EFI) for THEMIS, *Space Sci. Rev.*, *141*(1–4), 303–341, doi:10.1007/s11214-008-9469-2.

Engebretson, M., K. H. Glassmeier, M. Stellmacher, W. J. Hughes, and H. Lühr (1998), The dependence of high-latitude Pc5 wave power on solar wind velocity and on the phase of high-speed solar wind streams, *J. Geophys. Res.*, *103*(A11), 26,271–26,283, doi:10.1029/97JA03143.

Glassmeier, K. H. (1980), Magnetometer array observations of a giant pulsation event, *J. Geophys.*, *48*(3), 127–138.

Glassmeier, K. H., H. Volpers, and W. Baumjohann (1984), Ionospheric Joule dissipation as a damping mechanism for high-latitude ULF pulsations: Observational evidence, *Planet. Space Sci.*, *32*(11), 1463–1466, doi:10.1016/0032-0633(84)90088-6.

Greenwald, R. A., and A. D. M. Walker (1980), Energetics of long period resonant hydromagnetic-waves, *Geophys. Res. Lett.*, *7*(10), 745–748, doi:10.1029/GL007i010p00745.

Hardy, D. A., M. S. Gussenhoven, R. Raistrick, and W. J. McNeil (1987), Statistical and functional representations of the pattern of auroral energy flux, number flux, and conductivity, *J. Geophys. Res.*, *92*(A11), 12,275–12,294, doi:10.1029/JA092iA11p12275.

Junginger, H. (1985), Poynting vector as a diagnostic of hydromagnetic wave structure, *J. Geophys. Res.*, *90*(A5), 4155–4163, doi:10.1029/JA090iA05p04155.

Junginger, H., G. Haerendal, and F. Melzner (1985), A statistical study of wave Poynting vectors measured during long-period magnetospheric pulsations at geostationary orbit, *J. Geophys. Res.*, *90*(A9), 8301–8307, doi:10.1029/JA090iA09p08301.

Kouznetsov, I., and W. Lotko (1995), Radial energy transport by magnetospheric ULF waves: Effects of magnetic curvature and plasma pressure, *J. Geophys. Res.*, *100*(A5), 7599–7612, doi:10.1029/94JA02293.

Lee, D. H. (1996), Dynamics of MHD wave propagation in the low-latitude magnetosphere, *J. Geophys. Res.*, *101*(A7), 15,371–15,386, doi:10.1029/96JA00608.

Lee, D. H., and R. L. Lysak (1989), Magnetospheric ULF wave coupling in the dipole model: The impulsive excitation, *J. Geophys. Res.*, *94*(A12), 17,097–17,103, doi:10.1029/JA094iA12p17097.

Liu, J., V. Angelopoulos, D. Sibeck, T. Phan, Z. Y. Pu, J. McFadden, K. H. Glassmeier, and H. U. Auster (2008), THEMIS observations of the dayside traveling compression region and flows surrounding flux transfer events, *Geophys. Res. Lett.*, *35*, L17S07, doi:10.1029/2008GL033673.

McIlwain, C. E. (1966), Magnetic coordinates, *Space Sci. Rev.*, *5*(5), 585–598, doi:10.1007/BF00167327.

Mead, G. D., and D. H. Fairfield (1975), Quantitative magnetospheric model derived from spacecraft magnetometer data, *J. Geophys. Res.*, *80*(4), 523–534, doi:10.1029/JA080i004p00523.

Newton, R. S., D. J. Southwood, and W. J. Hughes (1978), Damping of geomagnetic pulsations by the ionosphere, *Planet. Space Sci.*, *26*(3), 201–209, doi:10.1016/0032-0633(78)90085-5.

Ozeke, L. G., I. R. Mann, and I. J. Rae (2009), Mapping guided Alfvén wave magnetic field amplitudes observed on the ground to equatorial electric field amplitudes in space, *J. Geophys. Res.*, *114*, A01214, doi:10.1029/2008JA013041.

Rae, I. J., et al. (2005), Evolution and characteristics of global Pc5 ULF waves during a high solar wind speed interval, *J. Geophys. Res.*, *110*, A12211, doi:10.1029/2005JA011007.

Rae, I. J., C. E. J. Watt, F. R. Fenrich, I. R. Mann, L. G. Ozeke, and A. Kale (2007), Energy deposition in the ionosphere through a global field line resonance, *Ann. Geophys.*, *25*(12), 2529–2539, doi:10.5194/angeo-25-2529-2007.

Sarris, T. E., W. Liu, X. Li, K. Kabin, E. R. Talaat, R. Rankin, V. Angelopoulos, J. Bonnell, and K. H. Glassmeier (2010), THEMIS observations of the spatial extent and pressure-pulse excitation of field line resonances, *Geophys. Res. Lett.*, *37*, L15104, doi:10.1029/2010GL044125.

Sibeck, D. G., and V. Angelopoulos (2008), THEMIS science objectives and mission phases, *Space Sci. Rev.*, *141*(1–4), 35–59, doi:10.1007/s11214-008-9393-5.

Tamao, T. (1965), Transmission and coupling resonance of hydromagnetic disturbances in the non-uniform Earth's magnetosphere, *Sci. Rep. Tohoku Univ. Ser.*, *5*, 43–72.

Zhu, X., and M. G. Kivelson (1991), Compressional ULF waves in the outer magnetosphere: 1.Statistical study, *J. Geophys. Res.*, *96*(A11), 19,451–19,467, doi:10.1029/91JA01860.

V. Angelopoulos and M. Hartinger, Earth and Space Sciences Department, University of California, 595 Charles E. Young Dr. East, Los Angeles, CA 90024, USA. (mhartinger@ucla.edu)

K.-H. Glassmeier, Institute for Geophysics and Space Physics, Technical University of Braunschweig, Mendelssohnstr. 3, D-38106 Braunschweig, Germany.

M. B. Moldwin, Atmospheric, Oceanic, and Space Sciences Department, University of Michigan, Space Research Building, 2455 Hayward St., Ann Arbor, MI 48109-2143, USA.

Y. Nishimura, Atmospheric and Oceanic Sciences Department, University of California, 405 Hilgard Ave., Los Angeles, CA 90095-1565, USA.